

# Optimal transport for multi-commodity routing on networks

Alessandro Lonardi,<sup>1,\*</sup> Enrico Facca,<sup>2</sup> Mario Putti,<sup>3</sup> and Caterina De Bacco<sup>1,†</sup>

<sup>1</sup>*Max Planck Institute for Intelligent Systems, Cyber Valley, Tübingen 72076, Germany*

<sup>2</sup>*Centro di Ricerca Matematica Ennio De Giorgi,*

*Scuola Normale Superiore, Piazza dei Cavalieri, 3, Pisa, Italy*

<sup>3</sup>*Department of Mathematics “Tullio Levi-Civita”,  
University of Padua, Via Trieste 63, Padua, Italy*

We present a model for finding optimal multi-commodity flows on networks based on optimal transport theory. The model relies on solving a dynamical system of equations. We prove that its stationary solution is equivalent to the solution of an optimization problem that generalizes the one-commodity framework. In particular, it generalizes previous results in terms of optimality, scaling, and phase transitions obtained in the one-commodity case. Remarkably, for a suitable range of parameters, the optimal topologies have loops. This is radically different to the one-commodity case, where within an analogous parameter range the optimal topologies are trees. This important result is a consequence of the extension of Kirkhoff’s law to the multi-commodity case, which enforces the distinction between fluxes of the different commodities. Our results provide new insights into the nature and properties of optimal network topologies. In particular, they show that loops can arise as a consequence of distinguishing different flow types, and complement previous results where loops, in the one-commodity case, were arising as a consequence of imposing dynamical rules to the sources and sinks or when enforcing robustness to damage. Finally, we provide an efficient implementation for each of the two equivalent numerical frameworks, both of which achieve a computational complexity that is more efficient than that of standard optimization methods based on gradient descent. As a result, our model is not merely abstract but can be efficiently applied to large datasets. We give an example of concrete application by studying the network of the Paris metro.

Optimizing networks for the distribution of quantities like passengers in a metro or data packets in a communication network, is a relevant matter for network planners. Similar problems arise in natural systems like river basins and vascular networks. A variety of models have been proposed to study these systems within an optimization framework [1–4]. The standard goal is finding the values of flow and conductivity that minimize a transportation cost. A common choice for this cost is the total power dissipation [1, 2, 5–7], but other types of costs can be defined based on the application, see for instance [8]. More recently, different approaches based on a dynamical adaptation of network properties coupled with conservation laws have been proposed [5, 6]. These models can be reformulated within the framework of optimal transport theory, following the work of [9–15]. Very efficient computational techniques have been developed for the solutions of these models [11–13]. Systems that follow adaptive rules can be mapped into a standard optimization setup [4, 5].

In all these natural systems there is a unique undistinguishable flow traveling through the network. However, in engineering networks like public transit networks, it is often the case that flows of different types compete for network infrastructure. In such applications, great costs are caused by traffic congestion or redundant capacity. Standard optimization approaches suffer of high computational costs caused by the simultaneous assignment of multiple interacting paths to minimize a global cost function. As a consequence, existing multi-commodity

flow algorithms rely on ignoring these interactions, or use greedy heuristics and approximations that lead to sub-optimal solutions [16]. Approaches based on statistical physics and message-passing algorithms have improved results [17, 18] but remain computationally costly.

In this Letter, we propose adaptation equations for multi-commodity flows that can serve as a simple physical explanation of the optimized network topologies found in engineering networks. We are inspired by the behavior of the slime mold *Physarum Polycephalum* [19], which uses a feedback mechanism between edge conductivities and flow to adapt its structure to changing nutrient patterns. We show that our dynamics can be mapped into a standard optimization framework that generalizes the one-commodity case. We derive the update equations for the algorithmic implementation of both approaches and empirically test their equivalence.

*Model* Consider a transportation network connecting a set  $\mathcal{V}$  of  $N$  stations (nodes) interconnected by a set  $\mathcal{E}$  of  $E$  links. Users enter and exit from a subset  $\mathcal{S} \subseteq \mathcal{V}$  of the stations, with  $|\mathcal{S}| = M \leq N$ . To model multi-commodity scenarios, we denote with  $g^i$  and  $h^i$  the number (or fraction) of users entering and exiting station  $i \in \mathcal{S}$ , respectively. To ensure global mass preservation, we assume that  $\sum_i g^i = \sum_i h^i$ . The indices  $i$  such that  $g^i > 0$  can be seen as “colors”, these allow to keep track of the station of origin and thus distinguish the flows of users based on it. Here we focus on transportation networks, but our model is applicable to all situations in which it is relevant to distinguish different flows, like multi-

commodities scenarios where different types of items are transported. For convenience, we define  $z_v^i$  as the number of users entering in  $i$  and exiting in  $v$  (we set  $z_v^i = 0$  if  $v \in \mathcal{V} \setminus \mathcal{S}$ ), thus  $\sum_{i \in \mathcal{S}} z_v^i = h^v$ . Note that while in general one might know  $g^i, \forall i \in \mathcal{S}$  (this is usually easier to track as users validate their ticket at the entrance), this might not be the case for  $z_v^i$  and  $h^i$ . We consider the realistic scenario where a user entering in one station cannot exit from the same one, thus avoiding trivial solutions. This means that  $z_v^i = 0$  for  $i = v$ . We denote with  $S_v^i = \delta_{iv} g^i - (1 - \delta_{iv}) z_v^i$  the source flux of color  $i$  in a source station  $v$ . Here and throughout the paper, the subscript  $v$  denotes the reference node and the superscript  $i$  the color. This implies that if a node  $v$  is a source for color  $i$ , it cannot be a sink for that color, i.e. the passengers cannot enter (exit) and exit (enter) in the same station. Instead, a station  $v \notin \mathcal{S}$  is a simple transit node and  $S_v^i = 0$  for all colors  $i$ . Let the ‘‘colored-flux’’  $F_e = (F_e^1, \dots, F_e^M)$  be a vector with entries  $F_e^i$ , which represent the number of users entered in station  $i \in \mathcal{S}$  who travel along edge  $e$ . In standard one-commodity cases, the flux per unit time could represent a water current or an electrical current and typically is ‘‘colorless’’, i.e.  $F_e$  is a scalar quantity. Denote with  $B$  the signed network incidence matrix, with entries  $B_{ve} = +1, -1$  if node  $v \in \mathcal{V}$  is the starting or ending point of edge  $e \in \mathcal{E}$ , respectively, and zero otherwise. We require the flux to obey the ‘‘colored’’ local Kirchoff’s law:

$$\sum_{e \in \mathcal{E}} B_{ve} F_e^i = S_v^i \quad \forall i \in \mathcal{S}, \forall v \in \mathcal{V} \quad , \quad (1)$$

where edges  $e = (u, v)$  have length  $\ell_e$ . We assume that the components (colors) of the flux derive from differences of a colored-potential (pressure) defined on nodes  $p_v^i$  and a colored-conductivity  $\mu_e^i$ :

$$F_e^i = \frac{\mu_e^i}{\ell_e} (p_u^i - p_v^i) \quad . \quad (2)$$

Up to this point, we have a set of independent one-commodity flows, one per color  $i$ . In realistic scenarios, the different colors interact, they use the same infrastructure and thus potentially create traffic congestion. We introduce interactions by imposing the constraint

$$\mu_e^i \stackrel{!}{=} \hat{\mu}_e \quad \forall e \in \mathcal{E}, \forall i \in \mathcal{S} \quad . \quad (3)$$

The quantity  $\hat{\mu}_e$  plays the role of a ‘‘colorless’’ conductivity. Given that the conductivity can be seen as proportional to the size of an edge, Eq. (3) can be interpreted as allocating the same edge capacity for the different colors. Notice, however, that the flux  $F_e^i$  still depends on the color, because the difference in potential does. This is one of the many possible choices of interaction between colors. While being analytically convenient, it allows for a rigorous generalization of the one-commodity case, as

we show below. We propose the following dynamics for the colorless conductivity:

$$\dot{\hat{\mu}}_e = \hat{\mu}_e^\beta \frac{\|\Delta P_{uv}\|_2^2}{\ell_e^2} - \hat{\mu}_e \quad \forall e \in \mathcal{E} \quad , \quad (4)$$

where we define  $\Delta P_{uv}$  as a vector of pressure differences with entries  $\Delta P_{uv}^i = p_u^i - p_v^i$  and  $\|\Delta P_{uv}\|_2^2 = \sum_{i \in \mathcal{S}} (p_u^i - p_v^i)^2$ . The parameter  $\beta$  determines the type of optimization associated to this dynamics. In the standard one-commodity case, for  $\beta < 1$  one aims at minimizing traffic congestion and obtains loopy topologies, for  $\beta > 1$  the aim is to consolidate paths and optimal topologies are trees; the case  $\beta = 1$  is shortest path-like. This dynamics describes a feedback mechanism. If the total flux through an edge is large, its conductivity increases. If the flux decreases, the conductivity decreases over time and becomes negligible when no flux occurs.

The systems of Eq. (1)-(4) represents our model for multi-commodity flow optimization. Notice that Eq. (4) couples together the various colors by means of the 2-norm of the pressure difference. Analogous one-commodity dynamics have been proposed to solve the basis pursuit problem on networks [13] and as a principled mechanism for filtering networks from redundancies [14]. More recently, similar ideas have been proposed for the shortest path-like case in multi-commodity [15]. Similarly to those cases, one can efficiently solve this system of equations using optimized numerical methods, however in our case the complexity increases with the number of colors, see Supplemental Material for more details [20]. Although not evident, our dynamics is connected with an optimization problem analogous to previous models for the one-commodity case [1, 2]. Specifically, the stationary solutions of our system minimizes the network total transportation cost  $J = \frac{1}{2} \sum_{e \in \mathcal{E}} \frac{\ell_e}{\hat{\mu}_e} \|F_e\|_2^2$  subject to the global constraint of constant material cost  $\sum_e \ell_e \hat{\mu}_e^{2-\beta} = K^{2-\beta}$  and local Kirchoff’s law on nodes as in Eq. (1). This optimization setup is analogous to that in [2], except here the flux appears in terms of its 2-norm. As in the one-commodity case, this leads to an optimal configuration where the conductivities similarly scale with the flux

$$\hat{\mu}_e \sim \|F_e\|_2^{2/(3-\beta)} \quad , \quad (5)$$

and the proportionality constant can be fully determined analytically (see Supplemental Material for detailed derivations [20]). Thus we can rewrite the total transportation cost in terms of the flux as

$$J_\Gamma = \sum_{e \in \mathcal{E}} \ell_e \|F_e\|_2^\Gamma \quad , \quad (6)$$

where  $\Gamma = 2(2 - \beta)/(3 - \beta)$ , which is analogous to the optimization problem of Banavar et al. [1] where there was no conductivity in the setup. Notice that all these results generalize the one-commodity case [1, 2] by means

of the 2-norm  $\|F_e\|_2$  of the colored flux. If there were only one color, and thus  $\|F_e\|_2^2 = F_e^2$ , our model reduces exactly to them. Solving this optimization problem directly by means of gradient descent is computationally expensive (see Supplementary Material [20]). Methods relying on Monte Carlo schemes [2] can also be computationally demanding and they are valid only when the optimal topology is known to be a tree. Instead, we analytically derive efficient update rules which have similar complexity as that of finding the steady states of our dynamics and can be implemented with efficient numerical solvers. They consist in iterating between updating conductivities and fluxes as follows:

$$\hat{\mu}_e = \frac{\|F_e\|_2^{2/(3-\beta)}}{\left(\sum_e \ell_e \|F_e\|_2^{2(2-\beta)/(3-\beta)}\right)^{1/(2-\beta)}} K \quad , \quad (7)$$

$$F_e^i = \frac{\hat{\mu}_e}{\ell_e} (p_u^i - p_v^i) \quad , \quad (8)$$

complemented with Kirchoff's law of Eq. (1), and can be put within the framework of fixed-point iterations. This generalizes results obtained adopting a similar approach for the one-commodity case [2, 3]. We make available an open source implementation of the two approaches which we summarize here: finding the steady state of the dynamics by solving the systems of Eq. (1)-(4) (Dynamics); extracting the solution of the optimization problem with the iterative updates of Eq. (7)-(8) (Optimization). They have similar computational complexity that scales as  $\mathcal{O}(M N^2)$ , and are much faster than techniques based on gradient descent, see Supplementary Material [20].

*Optimal topologies may have loops* Now we address the important question of which structures have the optimal topologies. For the analogous models in the one-commodity case, there is a phase transition at  $\beta = 1$  where optimal networks pass from being trees ( $1 < \beta < 2$ ) to containing loops ( $0 < \beta < 1$ ) [1, 2]. Remarkably, we obtain that in the multi-commodity case, loopy structures can be optimal also in the regime where trees were optimal in the previous models, depending on the values and locations of sources  $S_v^i$  and the edge lengths  $\ell_e$ . The first quantities are usually arbitrarily decided as input, while the latter are given by the system and cannot be tuned. Specifically, there exists a  $\beta^* \in (1, 2)$  such that we have a phase transition between trees and loopy structures. The value of  $\beta^*$  depends on  $(\{S_v^i\}, \{\ell_e\})$ . To illustrate this, consider the simple network of three nodes shown in Fig. 1. In this toy model, if we consider a particular choice of the fluxes, loopy structures can be optimal, i.e. they may be characterized by a lower value of  $J_\Gamma$  than trees. The loopy structures in what was previously a tree-like regime arise from the colored Kirchoff's law (1) distinguishing different colors entering and exiting a node. Had we imposed a similar but "colorless" constraint  $\sum_i \sum_{e \in \mathcal{E}_v} F_e^i = \sum_i S_v^i$ , trees would have been optimal. This can be seen by using a proof similar to that of Xia

[21] who used it for the one-commodity case. In fact, such proof does not always hold in the multi-commodity case when imposing the colored-constraint (see Supplementary Material [20] for details).

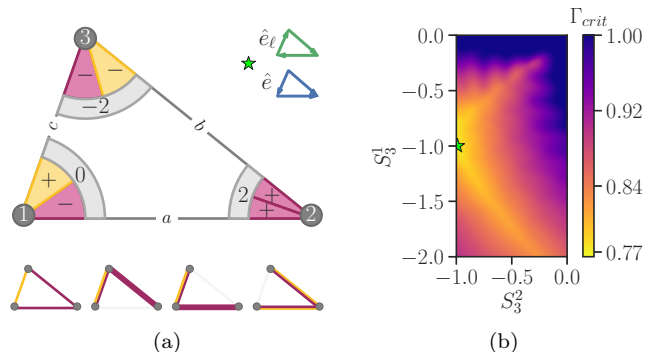


FIG. 1. Toy model where loops are optimal. (a) Sources/sinks are  $S_1 = (+1, -1, 0)$ ,  $S_2 = (0, +2, 0)$ ,  $S_3 = (-1, -1, 0)$ , so that there are in total 3 users entering from 2 stations, we distinguish the components of the fluxes on the edges with two colors; the numbers in the grey area inside the corners denote the net flux at nodes  $\sum_i S_v^i$ ;  $\ell_a = \ell_b = 1.5$ ,  $\ell_c = 1$ . On the bottom we show one loopy solution on the left and three trees on the right. The transportation cost of the loopy solution is lower than that of any of the trees for  $\Gamma \geq \Gamma_{crit} \simeq 0.83$ . The green and blue arrows denote the orientation of the loop and edges respectively. Specifically, the loops has fluxes  $F_a = (0, -1)$ ,  $F_b = (0, -1)$ ,  $F_c = (-1, 0)$ , the leftmost tree has  $F_a = (0, 0)$ ,  $F_b = (0, -2)$ ,  $F_c = (-1, 0)$  (similarly for the other two). (b) An example of a phase diagram that can be numerically found by fixing  $\ell_e$  as before,  $S_1^2 = -1 - S_3^1$ ,  $S_1^1 = -2 - S_3^2$ , while varying  $S_3^1$  and  $S_3^2$  ( $S_3^3 = 0, \forall v$ ). Notice that here we consider, more generally, real-valued entries. These can be interpreted as fractions of users entering/exiting from stations. The colorbar denotes the value of  $\Gamma_{crit}$  above which optimal solutions can be loopy. The green star is the configuration used in (a).

*Empirical results on the Paris metro* We apply our model to the metro of Paris [22]. The number  $g^i$  of users entering in a station  $i$  is assigned using the network manager open data [23], while the number  $z_v^i$  of users traveling from  $i$  to  $v$  is estimated based on  $g^i$ , as there are no open data for it. To this aim, we assign a positive number of passengers entering in each of the stations, i.e.  $g^i > 0, \forall i \in \mathcal{V}$ . After pre-processing, the network has a total of  $N = 302$  nodes and  $E = 359$  edges, coherently with the observed metro of Paris (see Supplementary Information [20] for details on data pre-processing and assignation of the users). We calculate the solutions of our model using both proposed approaches. As we can see from Fig. 2, where edge thickness is proportional to flux intensity, network topologies change from loopy to more tree-like structures as we vary  $\Gamma$ , as expected. The change in topology between different values of  $\Gamma$  is less evident for  $\Gamma > 1$ , than for  $\Gamma < 1$ . In fact, while

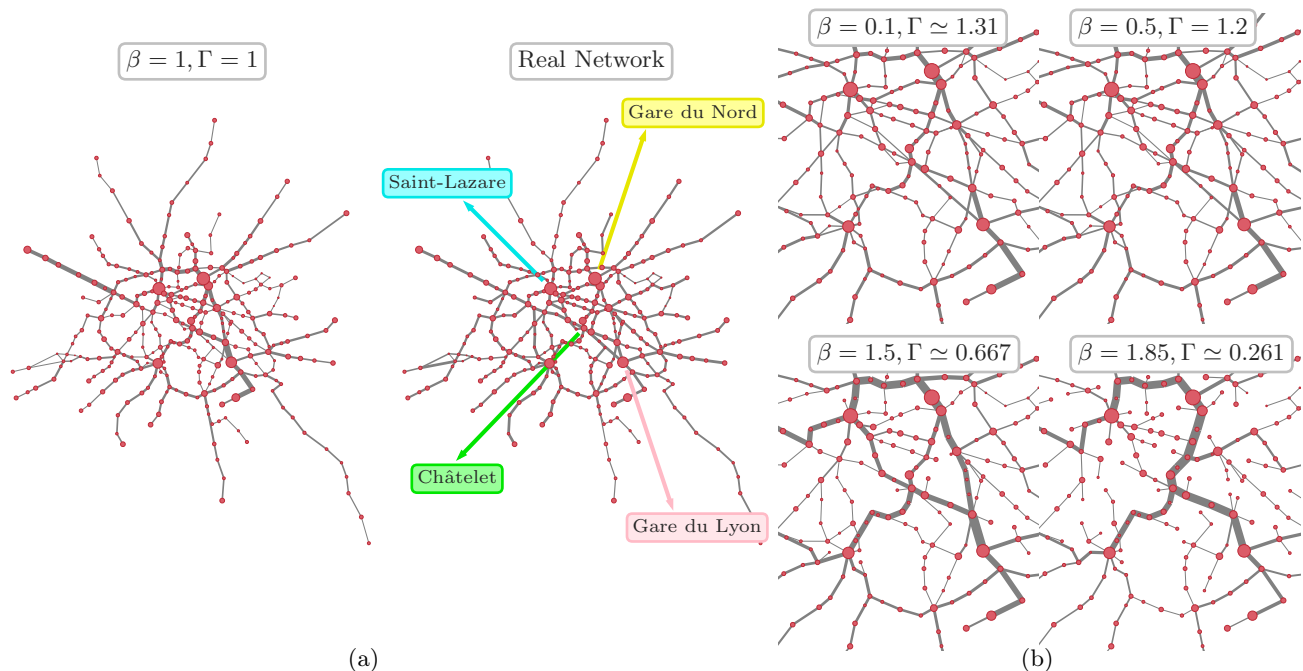


FIG. 2. Paris metro. Solutions of our model (Dynamics) for various optimization frameworks, set by tuning  $\beta$ . Edge thickness is proportional to the norm of the optimal values of the fluxes  $\|F_e\|_2$ . (a) On the left we show the network obtained fixing  $\beta = 1$ , i.e. shortest path-like. The rightmost figure is the original Paris network, edge thickness in this case is estimated accounting for the number of vehicles passing through each edge as reported in [22]. (b) Figures obtained varying  $\beta$  and zooming in to highlight the most congested part of the network, i.e. the city center.

the two top figures of Fig. 2b, relative to  $\Gamma = 1.2, 1.31$ , are very similar with traffic fairly uniform, we notice a significant difference between the two bottom configurations that are relative to  $\Gamma = 0.26, 0.67$ . Zooming into the city center, the latter figures show a non trivial difference in what is the main central artery, as this changes from having two routes branching from “Châtelet” connecting the stations of “Gare du Nord” and “Saint-Lazare” to “Gare de Lyon” to having one unique branch that goes from “Gare de Lyon” to “Saint-Lazare” via “Gare du Nord”. This behavior can be influenced by the existence of many local minima, as the cost function is not convex and both implementations converge to a possibly different local minimum, depending on the initial condition. We test for this by running the algorithm for different initializations of the conductivities selected uniformly at random. We found that, for any given value of  $\beta$ , our methods converge to configurations that differ only on a small fraction of the edges and have similar cost. Finally, we compared our solutions with the fluxes observed on the real network. We use as proxy the number of vehicles passing per day on each edge, a quantity reported in the dataset. The resulting network is shown on the right of Fig. 2a. The solutions for  $\Gamma > 1$  seem more aligned to the observations, with traffic uniformly distributed on the less congested main arteries. This suggests that network managers are optimizing for diminishing traffic conges-

tion and increasing robustness, rather than minimizing cost for building the infrastructure, which would be the main contribution for  $\Gamma < 1$ . Varying  $\Gamma$  continuously, we investigate how the topology finely changes by measuring the fraction of idle edges  $f_{idle}$ , defined as the ratio of edges with negligible flux over the total number of edges. As we can see in Fig. 3, this quantity monotonically decreases as  $\Gamma$  increases, i.e. as we transition from more tree-like structures to loopy ones. To get a better perspective of this, we compare these results with the solution obtained for a “one-commodity” scenario where we fix one station as the only source, and all the others as sinks. In this case,  $f_{idle}$  is constant up to a certain value around  $\Gamma = 1$  and then quickly decreases to zero. There seems to be a sharper transition from trees to loops, while for the multi-commodity case the process is smoother, and in fact solutions are not trees for the plotted values of  $\Gamma < 1$ . This is shown by the behavior of the number of basis loops (Fig. 3, inset), which shows that this number is non zero for a range of values when  $\Gamma < 1$ , i.e. solutions are not trees, while it is always zero for the one-commodity case, i.e. solutions are trees.

*Conclusions* Our model for multi-commodity routing on networks shows how optimal topologies with different structures can arise from simple dynamical rules. Generalizing our dynamics to account for interactions between commodities beyond the one proposed here and inves-



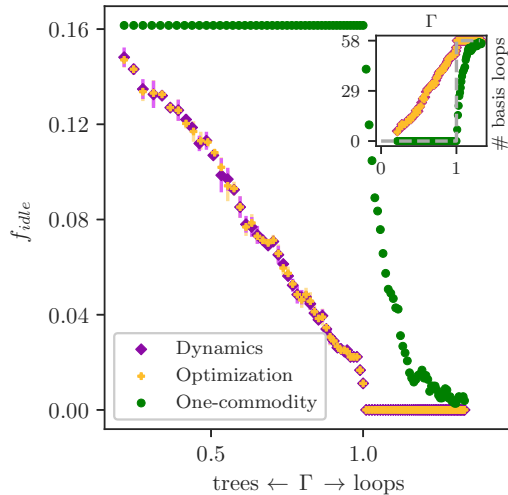


FIG. 3. Idle edges and loops. Fraction of idle edges  $f_{idle}$  in the Paris metro for various values of  $\Gamma$  (or  $\beta$ ). The circle green markers denote the curve obtained for the one-commodity case, i.e. considering one source and all the other sinks; in this case, solutions of the dynamics and optimizations coincide, we only show one marker. Error bars for the the one-source case are computed calculating standard deviations over 5 realizations permuting sources and sinks; in the multi-commodity case they are computed over 5 runs of the algorithm, each with different initial conductivities. When not shown, these are smaller than the marker size. The inset shows the number of basis loops.

tigating possible mappings to suitable optimization setups are natural next steps. While the discussion has been presented in terms of transportation networks, our model is broadly applicable beyond this setting, including all situations where it is relevant to distinguish flow types and to consider how these interact. One important example of such an instance is in communication networks where packets of information need to be delivered at different destinations. The insights gained about the structure of optimal topologies and the developed methods will open the way to further studies targeting these types of systems. To facilitate this, we provide an open source implementation of our code at <https://github.com/aleable/McOpt>.

We thank Kurt Mehlhorn for useful discussions and acknowledge the help of Daniela Leite for data pre-processing.

\* [alessandro.lonardi@tuebingen.mpg.de](mailto:alessandro.lonardi@tuebingen.mpg.de)

† [caterina.debacco@tuebingen.mpg.de](mailto:caterina.debacco@tuebingen.mpg.de)

[1] J. R. Banavar, F. Colaiori, A. Flammini, A. Maritan, and A. Rinaldo, *Phys. Rev. Lett.* **84**, 4745 (2000).

- [2] S. Bohn and M. O. Magnasco, *Phys. Rev. Lett.* **98**, 088702 (2007).
- [3] F. Corson, *Phys. Rev. Lett.* **104**, 048703 (2010).
- [4] K. Sinclair and R. C. Ball, *Phys. Rev. Lett.* **76**, 3360 (1996).
- [5] D. Hu and D. Cai, *Phys. Rev. Lett.* **111**, 138701 (2013).
- [6] H. Ronellenfitch and E. Katifori, *Phys. Rev. Lett.* **117**, 138301 (2016).
- [7] E. Katifori, G. J. Szöllösi, and M. O. Magnasco, *Phys. Rev. Lett.* **104**, 048704 (2010).
- [8] J. B. Kirkegaard and K. Sneppen, *Phys. Rev. Lett.* **124**, 208101 (2020).
- [9] V. Bonifaci, K. Mehlhorn, and G. Varma, *Journal of Theoretical Biology* **309**, 121 (2012).
- [10] F. Santambrogio, *Interfaces and Free Boundaries* **9**, 149 (2007).
- [11] E. Facca, F. Cardin, and M. Putti, *SIAM Journal on Applied Mathematics* **78**, 651 (2016).
- [12] E. Facca, S. Daneri, F. Cardin, and M. Putti, *Journal of Scientific Computing* **82**, 68 (2020).
- [13] E. Facca, F. Cardin, and M. Putti, [arXiv:1811.12691](https://arxiv.org/abs/1811.12691).
- [14] D. Baptista, D. Leite, E. Facca, M. Putti, and C. De Bacco, [arXiv:2005.02805](https://arxiv.org/abs/2005.02805).
- [15] V. Bonifaci, E. Facca, F. Folz, A. Karrenbauer, P. Kolev, K. Mehlhorn, G. Morigi, G. Shahkarami, and Q. Vermande, [arXiv:2009.01498](https://arxiv.org/abs/2009.01498).
- [16] K. Salimifard and S. Bigharaz, *Operational Research* (2020), [10.1007/s12351-020-00564-8](https://doi.org/10.1007/s12351-020-00564-8).
- [17] C. H. Yeung, D. Saad, and K. Y. M. Wong, *Proceedings of the National Academy of Sciences* **110**, 13717 (2013).
- [18] C. H. Yeung and D. Saad, *Journal of Physics A Mathematical and Theoretical* **46**, 103001 (2013).
- [19] A. Tero, S. Takagi, T. Saigusa, K. Ito, D. P. Bebber, M. D. Fricker, K. Yumiki, R. Kobayashi, and T. Nakagaki, *Science* **327**, 439 (2010).
- [20] See Supplemental Material for details about numerical implementation, theoretical proofs and discussion about Kirchoff's laws.
- [21] Q. Xia, *Communications in Contemporary Mathematics* **5**, 251 (2003).
- [22] R. Kujala, C. Weckström, R. K. Darst, M. N. Mladenović, and J. Saramäki, *Scientific data* **5**, 180089 (2018).
- [23] "Trafic annuel entrant par station du réseau ferré 2019", accessed: 2020-08-28 (2019).
- [24] W. L. Briggs, V. E. Henson, and S. F. McCormick, *A multigrid tutorial* (SIAM, 2000).

SUPPLEMENTARY INFORMATION (SI)

MAPPING THE DYNAMICS TO AN OPTIMIZATION PROBLEM

We argue that the stationary state of our dynamics can be mapped into the solution of an optimization problem which generalizes previous results obtained for one-commodity. First we show the existence of a scaling relationship between  $\hat{\mu}_e$  and  $\|F_e\|_2^2$  for the stationary state of our dynamics, always under the assumption that in each edge the conductivity per unit length is independent of the specific commodity. Consider the dynamics

$$\dot{\hat{\mu}}_e = \hat{\mu}_e^\beta \frac{\|\Delta P_{uv}\|_2^2}{\ell_e^2} - \hat{\mu}_e \quad \forall e = (u, v) \in \mathcal{E} \quad . \quad (\text{S1})$$

Setting the derivative on the left-hand-side to zero and recalling that  $F_e^i = \hat{\mu}_e (p_u^i - p_v^i) / \ell_e$  yields, for each edge

$$\hat{\mu}_e^{1-\beta} = \frac{\sum_i (p_u^i - p_v^i)^2}{\ell_e^2} = \sum_i \left( \frac{\ell_e F_e^i}{\hat{\mu}_e} \right)^2 \frac{1}{\ell_e^2} \quad (\text{S2})$$

$$\hat{\mu}_e^{3-\beta} = \|F_e\|_2^2 \quad . \quad (\text{S3})$$

This result is also supported by numerical simulations as shown in Fig. S1.

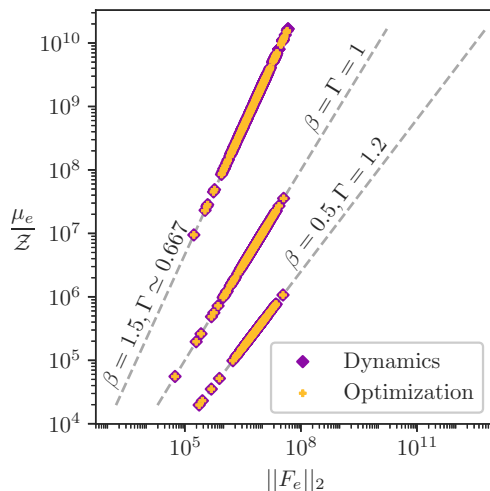


FIG. S1. Scaling between conductivity and flow. Empirical results on the Paris metro of the scaling law of Eq. (S3), for various  $\beta$ . The two approaches, dynamics and optimization, give same results. Dashed lines are the theoretical curves representing the exponent  $2/(3-\beta)$ , they perfectly fit with the empirical results. On the  $y$ -axis we normalize the conductivities computed using the Optimization method, i.e. iterating Eq. (S11), by  $Z = \frac{1}{(\sum_e \ell_e \|F_e\|_2^{2(2-\beta)/(3-\beta)})^{1/(2-\beta)}} K$ , so that we can obtain exactly Eq. (S3);  $K$  is an arbitrary constant, we set it to 1 in all our experiments.

Second, we show that a constrained optimization problem with a cost function representing the total dissipated energy over the whole network has a solution with the same scaling of Eq. (S3). Formally, consider the network dissipated energy:

$$J(\{\hat{\mu}_e\}, \{F_e\}) = \frac{1}{2} \sum_e \frac{\ell_e}{\hat{\mu}_e} \|F_e\|_2^2 \quad , \quad (\text{S4})$$

where  $\hat{\mu}_e$  is a scalar and  $F_e = (F_e^1, \dots, F_e^M)$ . In addition, we consider a global constraint on the conductivities  $\sum_e \ell_e \hat{\mu}_e^{2-\beta} = K^{2-\beta} > 0$ ,  $\beta \neq 2$ , and local (“colored”) Kirchoff’s laws on nodes

$$\sum_{e \in \mathcal{E}} B_{ve} F_e^i = S_v^i \quad \forall i \in \mathcal{S}, \forall v \in \mathcal{V} \quad , \quad (\text{S5})$$

where  $B_{ve}$  is the entry of the signed network incidence matrix. The problem can be turned into an unconstrained optimization problem by introducing Lagrange multipliers:

$$J_\beta(\{\hat{\mu}_e\}, \{F_e\}) = \frac{1}{2} \sum_e \frac{\ell_e}{\hat{\mu}_e} \|F_e\|_2^2 + \frac{\lambda}{2(2-\beta)} \left( \sum_e \ell_e \hat{\mu}_e^{2-\beta} - K^{2-\beta} \right) + \sum_{v,i} \chi_v^i \left( \sum_{e \in \mathcal{E}} B_{ve} F_e^i - S_v^i \right) . \quad (\text{S6})$$

Here we introduced a multiplicative factor  $1/2(2-\beta)$  for the Lagrange multiplier  $\lambda$  to ease calculations. Taking the partial derivatives w.r.t.  $\hat{\mu}_e$  and setting them to zero (the optimality condition on the derivative of  $J_\beta$  with respect to  $F_e$  will be treated later on):

$$\frac{\partial J_\beta(\{\hat{\mu}_e\}, \{F_e\})}{\partial \hat{\mu}_e} = -\frac{\ell_e}{2\hat{\mu}_e^2} \|F_e\|_2^2 + \frac{\lambda}{2} \ell_e \hat{\mu}_e^{1-\beta} \stackrel{!}{=} 0 \quad (\text{S7})$$

yields, for each edge,

$$\lambda \hat{\mu}_e^{3-\beta} = \|F_e\|_2^2 \quad \rightarrow \quad \hat{\mu}_e = \frac{1}{\lambda^{1/(3-\beta)}} \|F_e\|_2^{2/(3-\beta)} . \quad (\text{S8})$$

This is the same scaling relationship obtained from the stationary state of the dynamics in Eq. (S3), up to a multiplying constant. It is also the natural ‘‘colored’’ generalization of the one-commodity case presented in [1, 2, 5, 8], where instead of having  $\|F_e\|_2$  one has the absolute value  $|F_e|$ , as  $F_e$  is a scalar quantity there. Imposing the global constraint allows to determine the value of the multiplier  $\lambda$ :

$$\sum_e \ell_e \hat{\mu}_e^{2-\beta} = \sum_e \ell_e \frac{\|F_e\|_2^{2(2-\beta)/(3-\beta)}}{\lambda^{(2-\beta)/(3-\beta)}} = K^{2-\beta} \quad (\text{S9})$$

$$\lambda = \frac{1}{K^{3-\beta}} \left( \sum_e \ell_e \|F_e\|_2^{2(2-\beta)/(3-\beta)} \right)^{(3-\beta)/(2-\beta)} . \quad (\text{S10})$$

Substituting back into Eq. (S8) we obtain

$$\hat{\mu}_e = \frac{\|F_e\|_2^{2/(3-\beta)}}{\left( \sum_e \ell_e \|F_e\|_2^{2(2-\beta)/(3-\beta)} \right)^{1/(2-\beta)}} K \quad (\text{S11})$$

$$\hat{\mu}_e \sim (\|F_e\|_2^2)^{1/(1+\gamma)} , \quad (\text{S12})$$

which is analogous to that of the one-commodity case Eq. (5) in [2] for  $\gamma = 2 - \beta$ .

The total dissipation is obtained by substituting into Eq. (S4):

$$J = \sum_e \frac{\ell_e}{2K \|F_e\|_2^{2/(3-\beta)}} \|F_e\|_2^2 \left( \sum_e \ell_e \|F_e\|_2^{2(2-\beta)/(3-\beta)} \right)^{1/(2-\beta)} \quad (\text{S13})$$

$$= \frac{1}{2K} \sum_e \ell_e \|F_e\|_2^{2(2-\beta)/(3-\beta)} \left( \sum_e \ell_e \|F_e\|_2^{2(2-\beta)/(3-\beta)} \right)^{1/(2-\beta)} \quad (\text{S14})$$

$$= \frac{1}{2K} \left( \sum_e \ell_e \|F_e\|_2^{2(2-\beta)/(3-\beta)} \right)^{(3-\beta)/(2-\beta)} \quad (\text{S15})$$

$$= \frac{1}{2K} \left( \sum_e \ell_e \|F_e\|_2^{2\gamma/(1+\gamma)} \right)^{(1+\gamma)/\gamma} . \quad (\text{S16})$$

This is again analogous to that of the one-commodity case Eq. (6) in [2] for  $\gamma = 2 - \beta$ . Using similar arguments, i.e. noticing that the function  $x^{(3-\beta)/(2-\beta)} = x^{(1+\gamma)/\gamma}$  is monotonically increasing for  $0 < \gamma = 2 - \beta < 2$ , the original minimization problem reduces to that of minimizing with respect to  $\{F_e\}$  the cost:

$$J_\Gamma(\{F_e\}) = \sum_e \ell_e \|F_e\|_2^{2(2-\beta)/(3-\beta)} = \sum_e \ell_e \|F_e\|_2^\Gamma , \quad (\text{S17})$$

where  $\Gamma = 2(2 - \beta)/(3 - \beta) = 2\gamma/(1 + \gamma)$ , which is analogous to the model of Banavar et al. [1].

We can set to zero also the derivative w.r.t.  $F_e^i$  in Eq. (S6):

$$\frac{\partial J_\beta}{\partial F_e^i} = \frac{\ell_e}{\hat{\mu}_e} F_e^i + B_{ue} \chi_u^i + B_{ve} \chi_v^i \quad (\text{S18})$$

$$= \frac{\ell_e}{\hat{\mu}_e} F_e^i + B_{ue} (\chi_u^i - \chi_v^i) \stackrel{!}{=} 0 \quad , \quad (\text{S19})$$

$$\rightarrow F_e^i = -\frac{\hat{\mu}_e}{\ell_e} B_{ue} (\chi_u^i - \chi_v^i) \quad , \quad (\text{S20})$$

recovering the classical result stating that the pressures  $p$  is (minus) the Lagrange multiplier obtained when we minimize dissipated energy  $J(\{\hat{\mu}_e\}, \{F_e\})$  under the Kirchoff's laws constraints.

## OPTIMAL SOLUTIONS OF MULTI-COMMODITY FLOWS MAY HAVE LOOPS

Here we argue that optimal solutions of the multi-commodity problem are not necessarily trees. To do this we adapt to our ‘‘colored’’ case the proof of Proposition 2.1 in Xia [21], where it was shown that one-commodity (i.e., ‘‘colorless’’ Kirchoff’s law) optimal transport paths are trees, to show that in our case optimal solutions may contain loops. Our reasoning proceeds as follows. Each configuration of the edge flows  $\{F_e\}$  satisfying the ‘‘colored’’ Kirchoff’s law (Eq. (S5)) can be associated to a weighted graph  $\mathcal{G}(\mathcal{V}, \mathcal{E}, W)$  with weights  $w_e = \|F_e\|_2$ . Denote with  $\mathcal{T} = \mathcal{G}(\mathcal{V}, \mathcal{E}, W^*)$  the optimal tree topologies among these weighted graphs. Namely,

$$W^* = \{ \|F_e^*\|_2 : \left( F_e^* = \arg \min_{\{F_e\}} \{ J_\Gamma(\{F_e\}) \} \right) \wedge (\mathcal{G}(\mathcal{V}, \mathcal{E}, \|F_e^*\|_2) \text{ is a tree}) \} \quad . \quad (\text{S21})$$

These trees (not necessarily unique) can be obtained taking a weighted graph  $\mathcal{G}_L(\mathcal{V}, \mathcal{E}, W)$  with a single loop denoted as  $L$ , and cutting the loop by trimming one of its edges, then redistributing the fluxes passing through the trimmed edge over the remaining links of  $L$ . We assign an arbitrary orientation  $\hat{e}_\ell$  to the edges of  $L$  so that  $\langle \hat{e}_\ell, \hat{e} \rangle = \pm 1$ , where the direction  $\hat{e}$  of each link of a graph is uniquely determined by its incidence matrix. The edge to be cut is the one with smallest weight over the edges in the loop with a negative direction with respect to the graph’s orientation. Its flux is redistributed over the remaining edges, which now make a tree. Formally, we assign to the edges of  $\mathcal{T}$  fluxes  $F_e^*$  such that their entries are

$$(F_e^i)^* = F_e^i + \langle \hat{e}_\ell, \hat{e} \rangle F_{min}^i \quad \forall e \in \mathcal{E}, \forall i \in \mathcal{S} \quad , \quad (\text{S22})$$

with  $F_{min} = (F_{min}^1, \dots, F_{min}^M) = \arg \min_e \{ \|F_e\|_2 : \langle \hat{e}_\ell, \hat{e} \rangle = -1 \}$  and  $F_e$  are the fluxes of  $\mathcal{G}_L$ . The orientation of  $L$  can be switched in case the set of edges with negative orientation is empty. In the one-commodity case, as in Xia [21], there is a similar trimming, but with scalar weights on the tree being  $F_e^* = F_e + \langle \hat{e}_\ell, \hat{e} \rangle F_{min}$ , where now all the fluxes are scalar. The key effect of this is that  $F_e^*$  can become zero as a result of having a negative orientation  $\langle \hat{e}_\ell, \hat{e} \rangle$ ; in words, the flux  $F_{min}$  adds negatively to the fluxes originally present in  $\mathcal{G}_L$  along the edges in the loop with negative orientation, if  $F_{min} = F_e$  then  $F_e^* = 0$ . Here instead, in Eq. (S22) we add a vector. While we might have that for certain components the flux cancels out, the norm of the whole vector might not be zero, because not all the components cancel. This results from imposing a colored Kirchoff’s, and thus mass cannot all enter and exit from the same station. To illustrate this, we show this difference in a toy model triangle network in Fig. S2. The consequence is that now loops can be the optimal solutions while in the one-commodity case the optimal were trees.

### Toy model

We show in more detail a toy model that illustrates a simple example of a problem choice in which network with loops are more optimal than trees for  $0 < \Gamma < 1$ . Consider the simple triangular loop  $\mathcal{G}(\mathcal{V} = \{1, 2, 3\}, \mathcal{E} = \{a, b, c\})$  represented in Fig. S2a (top) with three nodes that are sources/sinks, i.e.  $\mathcal{S} \equiv \mathcal{V}$  and lengths  $\ell = (\ell_a, \ell_b, \ell_c)$ . We set  $g = (+1, +2, 0)$  so that  $S_1 = (+1, -z_1^2, 0)$ ,  $S_2 = (0, +2, 0)$ ,  $S_3 = (-1, -z_3^2, 0)$  (with  $z_1^2 + z_3^2 = +2$ ); in practice, we need to distinguish only two commodities, depicted in two different colors in the Figure, as  $g^3 = 0$ . For this simple case, Kirchoff’s law allows only for three possible tree topologies  $\mathcal{T}_i$ ,  $i = 1, 2, 3$ , these are shown on the bottom right of Fig. S2a. In detail, by solving Kirchoff’s law, we can write everything as a function of  $F_a = (F_a^1, F_a^2, 0)$ . Then,



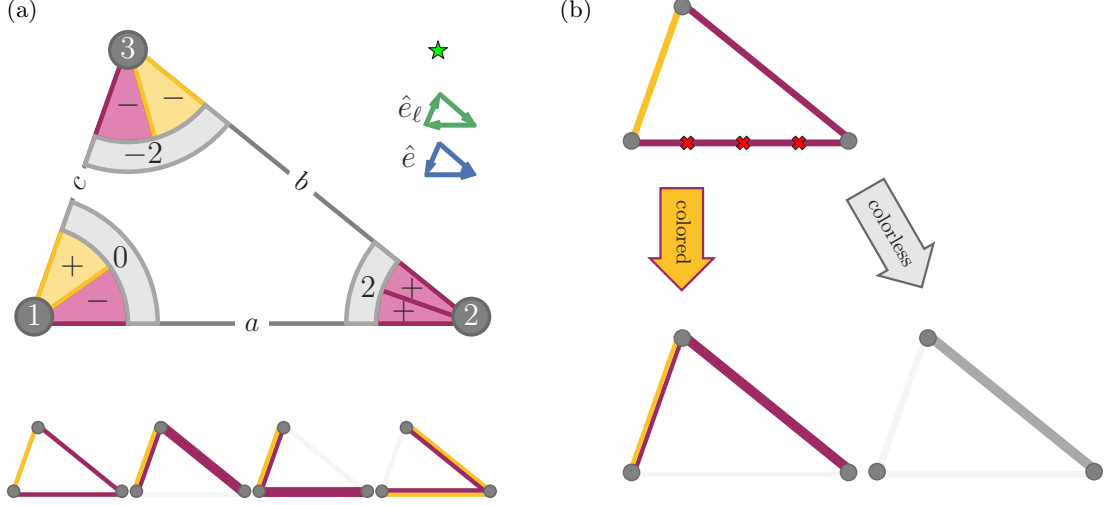


FIG. S2. (a) Toy model where loops are optimal. The triangle network has source vectors  $S_1 = (+1, -1, 0)$ ,  $S_2 = (0, +2, 0)$ ,  $S_3 = (-1, -1, 0)$ ,  $\ell_a = \ell_b = 1.5$ ,  $\ell_c = 1$ . On the bottom we show one loopy solution on the left and three trees on the right. The transportation cost of the loopy solution is lower than that of any of the trees, for  $\Gamma \geq \Gamma_{crit} \simeq 0.83$ . The green and blue arrows denote the orientation of the loop and edges respectively. Specifically, the loop has fluxes  $F_a = (0, -1)$ ,  $F_b = (0, -1)$ ,  $F_c = (-1, 0)$ , the leftmost tree has  $F_a = (0, 0)$ ,  $F_b = (0, -2)$ ,  $F_c = (-1, +1)$  (similarly for the other two). Their transportation costs are calculated using Eq. (S28)-(S30). (b) Applying the trimming procedure analogous to that used in Xia [21] for the one-commodity case, would mean redistributing the flux  $F_{min} = F_a$  of the least-weighted edge of the loop to the remaining edges. We would obtain the leftmost tree in the figure, which is not optimal for  $\Gamma \geq \Gamma_{crit}$ . If we forget about colors and consider the one-commodity case and apply the trimming exactly as in Xia [21], redistributing the flux (which is now a scalar quantity)  $F_{min} = F_a = -1$  on edge  $c$  would cancel out the first and second component, i.e.  $F_c^* = -1 - (-1) = 0$ , because we lose track of the colors. In this case then, the tree  $\mathcal{T}$  would have fluxes  $F_a^* = 0$ ,  $F_b^* = -2$ ,  $F_c^* = 0$  and thus lower cost  $J_{\mathcal{T}} = \frac{3}{2} 2^{\Gamma} \leq 4 = J_{loop}$  when  $0 < \Gamma \leq \log(8/3)/\log 2 \simeq 1.42$ . However, this would not comply with the colored Kirchoff's law anymore, as the first color trivially enters and exits from the same node 1.

by choosing two arbitrary values of  $F_a^1, F_a^2$  we propose a loopy solution  $\mathcal{G}_L$  to compare against the trees, this is the leftmost bottom triangle in Fig. S2a. We show that there are values of  $0 < \Gamma < 1$  for which this loopy solution has lower transportation cost than any of the trees. Computing all the costs using Eq. (S17) yields:

$$J_{\Gamma}(\mathcal{T}_1) = 2^{\Gamma} \ell_b + 2^{\Gamma/2} \ell_c \quad (\text{S23})$$

$$J_{\Gamma}(\mathcal{T}_2) = 2^{\Gamma} \ell_a + 2^{\Gamma/2} \ell_c \quad (\text{S24})$$

$$J_{\Gamma}(\mathcal{T}_3) = (\ell_a + \ell_b) 2^{\Gamma/2} \quad (\text{S25})$$

$$J_{\Gamma}(\mathcal{G}_L) = ((F_a^1)^2 + (F_a^2)^2)^{\Gamma/2} \ell_a + ((F_a^1)^2 + (F_a^2 + 2)^2)^{\Gamma/2} \ell_b + ((F_a^1 - 1)^2 + (F_a^2 + 1)^2)^{\Gamma/2} \ell_c \quad (\text{S26})$$

Thus, we need to find values of  $\{\ell^* = (\ell_a^*, \ell_b^*, \ell_c^*), F_a^*, \Gamma^*\}$  for which

$$J_{\Gamma}(\mathcal{G}_L; \ell^*, F_a^*, \Gamma^*) \leq \min\{J_{\Gamma}(\mathcal{T}_i; \ell^*, F_a^*, \Gamma^*) : i = 1, 2, 3\} \quad (\text{S27})$$

holds. To find an example solution, we could fix certain values for these parameters. In practice, the lengths are usually given in input, thus we set  $\ell_a = \ell_b = \frac{3}{2} \ell_c$ ,  $\ell_c = 1$ ; we then propose  $F_a^* = (0, -1, 0)$ . Thus:

$$J_{\Gamma}(\mathcal{T}_1) = J_{\Gamma}(\mathcal{T}_2) = \frac{3}{2} \times 2^{\Gamma} + 2^{\Gamma/2} \quad (\text{S28})$$

$$J_{\Gamma}(\mathcal{T}_3) = 3 \times 2^{\Gamma/2} \quad (\text{S29})$$

$$J_{\Gamma}(\mathcal{G}_L) = 4 \quad (\text{S30})$$

Analytically from Eq. (S28)-(S30) or numerically solving Eq. (S27) (fixing  $F_a^*$  as proposed for  $\mathcal{G}_L$ ) one can show that  $\Gamma^* \simeq 0.83$ . For  $\Gamma \geq \Gamma^*$ , the cost  $J_{\Gamma}(\mathcal{G}_L; \Gamma)$  is always optimal, i.e. we have a phase transition between trees to loopy optimal topologies. Notice that such values of  $\Gamma^*$  depend on the selected values of  $(\ell, F_a)$ , and that optimal loopy solutions are not guaranteed to exist for any arbitrary configuration of these values. This can be numerically

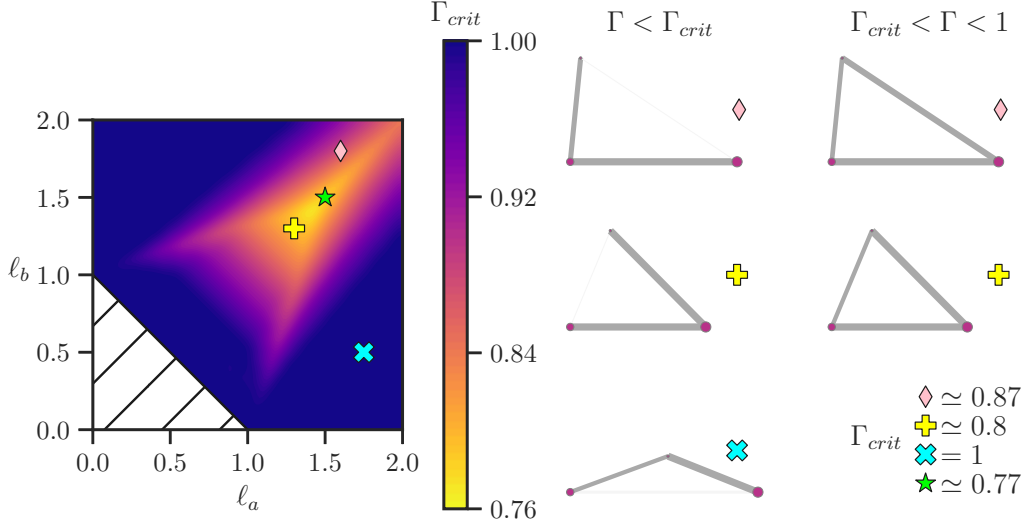


FIG. S3. Phase diagram tree-loopy optimal topologies.  $\Gamma_{crit}$  denotes the minimum value of  $\Gamma$  above which loops are more optimal than trees. The setup is the same as for the toy model in Fig. S2. Values of  $\Gamma_{crit}$  are found by solving Eq. (S27);  $\ell_c = 1$ . The area under the triangular surface in white background is not allowed as the triangular geometry is not defined in there. One can notice that there is an entire region where  $\Gamma_{crit} \leq 1$ , inside it loops are optimal. On the r.h.s of the Figure we show three different topologies, i.e. choices of  $\ell_a, \ell_b$  for which optimal solutions can be loopy; these are associated with the markers drawn on the heatmap, the green star is the configuration of the toy model in Fig (S2). In particular, running our dynamics on the pink-diamond graph (resp. the yellow-plus) leads to a loopy configuration for  $\Gamma > \Gamma_{crit}$  or to  $\mathcal{T}_2$  (resp.  $\mathcal{T}_3$ ) if  $\Gamma < \Gamma_{crit}$ ; width of the edges is proportional to the final  $\|F_e\|_2$ , the edges not visible have negligible fluxes; nodes dimensions are proportional to  $g$ . Running our dynamics on the blue-cross graph returns always  $\mathcal{T}_1$  since it  $\Gamma_{crit}$  is equal to 1. In the bottom right portion of the panel we report the values of  $\Gamma_{crit}$  obtained solving Eq. (S27) fixing  $\ell_a, \ell_b$  as given by the markers.

investigated using similarly reasoning as done for the case above. The important point here is that we could find *at least* one setting of  $(\ell, F_a)$  for which we have loopy solutions in the non-trivial regime  $0 < \Gamma < 1$ . Indeed, at  $\Gamma = \Gamma^*$  we have  $J_\Gamma(\mathcal{G}_L; \Gamma) = J_\Gamma(\mathcal{T}_1) = J_\Gamma(\mathcal{T}_2) = J_\Gamma(\mathcal{T}_3) = 4$ . Generalizing to other values of  $\ell_a, \ell_b$ , while fixing  $\ell_c = 1$ , one can (with similar reasoning) determine a phase diagram as in Fig. S3, where  $\Gamma_{crit}$  is obtained solving Eq. (S27) for different pairs  $(\ell_a, \ell_b)$ .

## NUMERICAL IMPLEMENTATION

### Pre-processing

The model is tested in the metro network of Paris. The network topology data are collected from [22], while the number of users exiting and entering each station are in [23]. The original dataset is provided as a multilayer network embedded with different transportation types, thus we performed a pre-processing to extract solely the metro network. The initial graph had originally 383 nodes, while the observed metro of Paris has 302 stations. In order to coherently remove duplicates we first trimmed the nodes belonging to other layers (transportation types). Then we merged redundant stations who have the same name, hence collapsing these nodes together. This redundancy was due to the presence in the original dataset of two entrances for the same stations located in slightly different geographical positions; the difference in coordinates was always negligible compared to the physical extension of the whole network. The trimmed network reflects more consistently the observed real topology and it is made of  $M = N = 302$  stations and  $E = 359$  edges. For convenience, longitude and latitude coordinates were both rescaled within the range  $[0, 1]$ . The entries of  $S$  are assigned based on the “importance” of each station, measured as the number of passengers entering in it. This assumption is necessary, as we do not have access to exact travel routes data. In practice, we assign  $M - 1$  positive “influence factors” to each station  $i$ , one for each node  $v$  in  $\mathcal{S} \setminus \{i\}$  where the users entering in  $i$  can potentially

exit:

$$r_v^i = \frac{g^v}{\sum_{u \in \mathcal{S} \setminus \{i\}} g^u} \quad \forall v \in \mathcal{S} \setminus \{i\} \quad , \quad (\text{S31})$$

instead  $r_i^i = 0$  and  $r_v^i = 0$  if  $v \in \mathcal{V} \setminus \mathcal{S}$ . Notice that  $r_v^i \in [0, 1]$  and  $\sum_{v \in \mathcal{V} \setminus \{i\}} r_v^i = 1$ . Thus, we can estimate the number of people exiting from a station  $v$ , by assigning  $z_v^i = r_v^i g^i$ ,  $\forall i \in \mathcal{S}$ ,  $v \in \mathcal{V}$  (respecting the convention  $z_v^i = 0$  if  $v \in \mathcal{V} \setminus \mathcal{S}$ ). The intuition is that a station  $v$  with high volume of passengers entering, i.e. high  $g^v$ , should also take a high volume of exiting ones which originated from other stations  $i$ , i.e. high ‘‘influence’’  $r_v^i$  and thus high  $z_v^i$ . This number in general can be real; however, if one wants to interpret it as the number of people traveling in a transportation system, one can simply assign its closest integer to it, for instance using the floor function. In this case, to insure mass balance, we conventionally redistribute residuals  $\varepsilon^i = g^i - \sum_{v \in \mathcal{V} \setminus \{i\}} z_v^i$  obtained because of the floor function to a random node  $v \in \mathcal{S} \setminus \{i\}$ .

### Numerical implementation

We propose two approaches to solve the multi-commodity problem: one based on the finding the steady state of the conductivities using Eq. (S1) (Dynamics), and one implementing the iterative update of Eq. (S11), (S19) and (S20) (Optimization). The implementations of these methods are summarized in Algorithms (1) and (2).

---

#### Algorithm 1 Dynamics

---

- 1: Input:  $\mathcal{G}(\mathcal{V}, \mathcal{E}) =$  adjacency list, nodes coordinates;  $\mathcal{S}; \{g^i\}; 0 < \beta < 2$
  - 2: Initialize: (i)  $S$  and (ii)  $\{\hat{\mu}_e\}$  (e.g. sampling as i.i.d.  $\hat{\mu}_e \sim U(0, 1)$ )
  - 3: **while** convergence not achieved **do**
  - 4:   solve Kirchoff’s law as in Eq. (S5)  $\rightarrow \{P_v^i\}$
  - 5:   update conductivities with a finite difference discretization of Eq. (S1):  $\{\hat{\mu}_e^t\} \rightarrow \{\hat{\mu}_e^{t+1}\}$
  - 6: **end while**
  - 7: Return: fluxes  $\{F_e^i\}$  at convergence, computed using  $F_e^i = \hat{\mu}_e(p_u^i - p_v^i)/\ell_e$ ,  $e = (u, v)$
- 

---

#### Algorithm 2 Optimization

---

- 1: Input:  $\mathcal{G}(\mathcal{V}, \mathcal{E}) =$  adjacency list, nodes coordinates;  $\mathcal{S}; \{g^i\}; 0 < \beta < 2$
  - 2: Initialize: (i)  $S$  and (ii)  $\{\hat{\mu}_e\}$  (e.g. sampling as i.i.d.  $\hat{\mu}_e \sim U(0, 1)$ )
  - 3: **while** convergence not achieved **do**
  - 4:   solve Kirchoff’s law as in Eq. (S5)  $\rightarrow \{P_v^i\}$
  - 5:   compute  $\hat{\mu}_e(F_e)$  using Eq. (S11)
  - 6:   update fluxes using Eq. (S19) and (S20)
  - 7: **end while**
  - 8: Return: fluxes  $\{F_e^i\}$  at convergence
- 

These pseudo-codes outline our methods, however practitioners can make further arbitrary choices about what numerical routines to use in the various steps. In our implementation, we solved  $M$  ordinary differential equations as in Eq. (S1) by means of an explicit Euler method, thus at each step the local truncation error is approximately proportional to  $\Delta t^2$ , with  $\Delta t$  being the difference between two consecutive time steps, which can be arbitrarily set in input. Solutions of Kirchoff’s law have been computed using a direct solver (UMFPACK). Lastly, we impose the following convergence criteria: *convergence* is achieved when these conditions are satisfied

$$\text{Dynamics: } \max_e |\hat{\mu}_e^{t+1} - \hat{\mu}_e^t| / \Delta t < \tau_{dyn}, \quad \text{Optimization: } \max_e \left| \|F_e\|_2^{t+1} - \|F_e\|_2^t \right| < \tau_{opt} \quad (\text{S32})$$

where  $\tau_{dyn}, \tau_{opt} > 0$  are parameters arbitrarily set in input. In our experiments we use  $\tau_{dyn} = 10^{-3}$ ,  $\tau_{opt} = 10^{-5}$ . To test our methods, we developed a momentum-based gradient descent as baseline algorithm. This consists in the component-wise iterative update of the fluxes using

$$(V_e^i)^t = \eta (\partial J_\beta / \partial F_e^i)^t + \delta (V_e^i)^{t-1} \quad (\text{S33})$$

$$(F_e^i)^{t+1} = (F_e^i)^t + (V_e^i)^t \quad (\text{S34})$$

with  $\eta, \delta > 0$  fixed increment rates and  $(V_e^i)^0 = F_e^i$ . We fixed the convergence criteria analogously to what done for the other two methods:  $\max_e \left| \|F_e\|_2^{t+1} - \|F_e\|_2^t \right| / \eta < \tau_{gd}$ , with  $\tau_{gd} > 0$  a parameter that needs to be set in input. In our experiments we set it to  $\tau_{gd} = 10^{-2}$ . After running our algorithms until convergence, the original network is trimmed by removing edges with negligible fluxes. Formally, we remove links for which  $\|F_e\|_2 < \tau$ , with  $\tau > 0$  arbitrarily fixed. Typically, as we empirically found, the distribution of  $\|F_e\|_2$  over the edges is divided in two sets with values of several order of magnitude different between the two sets. It is thus straightforward to distinguish what edges to be trimmed, i.e. those that have negligible values compared to the rest of the distribution.

*Computational complexity*

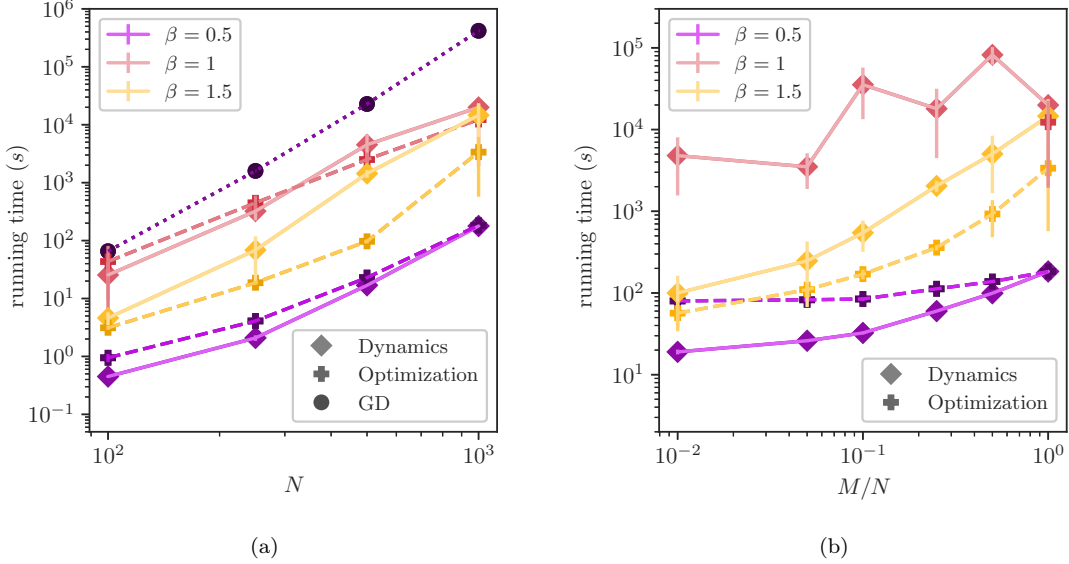


FIG. S4. Computational complexity. (a) Running time (in seconds) as a function of system size  $N$ . (b) Running time as a function of the ratio  $M/N$  between the number of commodities and system size. GD denotes gradient descent, implemented with Eq. (S33) and (S34); we only show it for  $\beta = 0.5$  as for the other values it fails to converge within a reasonable time. Similarly, for  $\beta = 1$  and  $M/N < 1$ , Optimization fails to converge, hence we only report Dynamics.

Each temporal step of the explicit Euler method executed in our algorithms requires the approximate solution of  $M$  linear systems of dimension  $N$ . This operation has been carried out by means of a sparse direct solver (UMFPACK) that performs a LU decomposition for each column of the right hand side of Eq. (S5). The total computational complexity of this process scales as  $\mathcal{O}(MN^2)$ . To have a better understanding of this we tested our models several synthetic Waxman networks obtained by placing  $N$  nodes uniformly at random in a square domain of size 1. Nodes are connected with probability  $p = A \exp(-d/\alpha L)$ , where  $A, \alpha, L$  are parameters that we fix arbitrarily to  $A = 1/4$ ,  $\alpha = 1/4$  and  $L = 1$ ;  $d$  is the euclidean distance between a pair of nodes. The matrix  $S$  is set by assigning a total in-flowing mass  $\sum_i g^i = 10^4$  at random among all the commodities and using the same “influence assignment” described by Eq. (S31). We test the efficiency of our algorithms by measuring the total running time (in seconds) to implement the algorithms for different values of  $\beta, M, N$ . Results are shown in Fig. S4. We notice that the two algorithms Dynamics and Optimization have similar computational complexity. Their small running time’s differences are negligible and only due to how convergence is precisely defined, i.e. how the corresponding parameters  $\tau_{dyn}, \tau_{opt}$  are set. The running time is shorter for  $\beta < 1$  (traffic optimization, loopy) than in the opposite scenario of  $\beta > 1$  (minimization of infrastructural cost, tree-like). The case  $\beta = 1$  is more nuanced, as the cost transitions between two opposite situations. In this case, Optimization fails to converge for  $M/N < 1$ , if convergence is defined in terms of variations of  $\|F_e\|_2$  between iteration steps. This is because the algorithm gets lost in degenerate local minima, configurations with same cost but different set of fluxes. This lack of convergence suggests that, for  $\beta = 1$ , the energy landscape around these minima is flat, i.e. there are many configurations with same cost but non-negligible differences

in their fluxes. The Optimization routine keeps switching between these different states. In this case, one can simply pick one of these possible many solution as an example local optima. The dynamics does instead converge. This suggests that Dynamics is biased towards one of these degenerate solutions. For  $M/N = 1$ , Optimization converges with same running time as Dynamics, suggesting that, in this case, as we increase  $M$  the landscape becomes less flat. A possible cause is that by increasing  $M$  the system has more constraints to be satisfied via Kirchoff's law, which reduces the number of possible degenerate solutions. This claim is also supported by the behavior of Dynamics' running time, which does not monotonically increase with  $M/N$  in this case, as shown in Fig. S4b. These behaviors highlight relevant differences between the two implementations. Finally, we note that the computational complexity could in principle be further reduced to  $\mathcal{O}(M N)$  using multigrid methods [24], we do not explore this here.

---